HHS Public Access

Author manuscript

Nat Immunol. Author manuscript; available in PMC 2016 May 01.

Published in final edited form as:

Nat Immunol. 2015 November ; 16(11): 1162–1173. doi:10.1038/ni.3288.

Control of peripheral tolerance by regulatory T cell-intrinsic Notch signaling

Louis-Marie Charbonnier[1], **Sen Wang**[1], **Peter Georgiev**[1], **Esen Sefik**[2], and **Talal A Chatila**[1]

[1]Division of Immunology, Boston Children's Hospital, Department of Pediatrics, Harvard Medical School, Boston, MA 02115, U.S.A

[2]Division of Immunology, Department of Microbiology and Immunobiology, Harvard Medical School, Boston, Massachusetts 02115 U.S.A

Abstract

Notch receptors direct the differentiation of T helper (T_H) cell subsets, but their influence on regulatory T (T_{reg}) cell responses is obscure. We here report that lineage-specific deletion of components of the Notch pathway enhanced T_{reg} cell-mediated suppression of T_H1 responses, and protected against their T_H1 skewing and apoptosis. Expression in T_{reg} cells of gain of function transgene encoding Notch1 intracellular domain resulted in lymphoproliferation, exacerbated T_H1 responses and autoimmunity. Cell-intrinsic canonical Notch signaling impaired T_{reg} cell fitness, promoted the acquisition by T_{reg} cells of a T_H1 cell-like phenotype, whereas Rictor-dependent non-canonical Notch signaling activated the AKT-Foxo1 axis and impaired *Foxp3* epigenetic stability. These findings establish a critical role for Notch signaling in controlling peripheral T_{reg} cell functions.

Notch signaling serves pleiotropic roles in the immune system by influencing multiple lineage decisions of developing lymphoid and myeloid cells [1, 2]. In mammals, the Notch family is composed by 4 Notch receptors (Notch1–4) and 5 ligands (Delta-like1, 3, and 4 and Jagged1 and 2). After ligand-receptor interaction, the intracellular domain of the Notch receptor is cleaved, traffics to the nucleus and forms complexes with the DNA binding factor RBPJ and the transcriptional co-activators MAML1-3, promoting expression of target genes. In addition to this canonical pathway, cleaved intracellular domains of Notch receptors engage non-canonical signaling components, including the metabolic checkpoint kinase complex mTORC2 and its associated adaptor Rictor [3, 4]. Notch intracellular domain also interacts with components of the NF-κB, TGF-β and the hypoxia response pathways [5, 6, 7].

Correspondence should be addressed to T.A.C (talal.chatila@childrens.harvard.edu).

Author Contributions

L-M.C. and T.A.C. designed the experiments and evaluated the data; L-M.C., S.W., P.G. and E.S. performed experiments; L-M.C. and E.S. analyzed data and prepared the Figures, T.A.C. conceived of the project and directed the research, L-M.C. and T.A.C. wrote the manuscript.

Accession Codes. Gene Expression Omnibus GSE71343.

Notch signaling is activated at various stages of commitment and development of T cell lineages, such as commitment to the T cell versus the B cell lineage, αβ versus γδ T cell differentiation and CD4 T versus CD8 single-positive T cell differentiation [1, 2], and during T cell-mediated immune responses, such as peripheral cytotoxic and helper T (T_H) cell differentiation and function [8]. Pathogen-associated molecular patterns are known to promote expression of Notch ligand at the surface of antigen presenting cells. Activation of naive $CD8^+$ T cells requires binding of Delta-like1 on antigen presenting cells by Notch1 or Notch2 leading to expression of *Eomes*, *Gzmb*, *Ifng* and *Pfr1* [9, 10]. In naïve $CD4^+$ T cells, Delta-like1 and 4 activate Notch signaling and *Tbx21* transcription, encoding the T_H1 transcriptional regulator T-bet [11, 12]. During T_H2 differentiation, activation of Notch1 and 2 by Jagged1 and Jagged2 favor the expression of *Gata3* and *Il4* [13, 14, 15, 16].

Notch1 signaling has been described to be important in the differentiation of T_H17 and T_H9 subsets of helper T cells by promoting *Rorc* and *Il9* expression, respectively [5, 17, 18]. The role of Notch signaling in the regulatory T (T_{reg}) cell compartment remain controversial. *In vitro*, Jagged ligands and Notch 1 and Notch3 signaling seem to promote T_{reg} cell differentiation and survival [3, 19, 20, 21]. In contrast, several *in vivo* studies have demonstrated that blockade of the Notch pathway, in particular Notch1 and Notch2, promotes tolerance in murine models of graft versus host disease, in association with the expansion of T_{reg} cells [22, 23]. Studies have shown tolerogenic functions for antibodies to Notch1 in a humanized mouse model of vasculitis and in a murine model of aplastic anemia [24, 25]. In this study, we have employed T_{reg} cell lineage-specific genetic and functional approaches to identify a key role for the Notch pathway in destabilizing T_{reg} cells, promoting their apoptosis and inhibiting their function in the context of inflammation.

Results

Notch negatively regulates T_{reg} cell functions and homeostasis

To elucidate the role of the Notch pathway in peripheral tolerance, we examined the functional consequences of interrupting Notch receptor signaling in a T_{reg} cell-specific manner. To this end, we derived mice with a bacterial artificial chromosome (BAC) expressing an enhanced green fluorescent protein fused with the Cre recombinase under the control of Foxp3 promoter together with *lox*P-flanked *Pofut1*, encoding the enzyme protein O-fucosyltransferase 1 (called *Foxp3*^{EGFPCre}*Pofut1*$^{Δ/Δ}$ here; Supplementary Fig. 1a, b) [26]. The latter mediates fucosylation of Notch receptors, which is essential for receptor ligand interaction; its deficiency abrogates Notch signaling [26]. T_{reg} cell-specific Pofut1 deficiency resulted in a decrease in peripheral $CD3^+$ T cells and $CD4^+$ T cell numbers by about 25% compared to *Foxp3*^{EGFPCre} mice (Fig. 1a). It also resulted in a reciprocal increase in T_{reg} cell frequency, with decreased $CD4^+CD62L^{lo}CD44^{hi}$ T effector memory and a relative increase in $CD62L^{hi}CD44^{lo}$ naïve T cells as compared to *Foxp3*^{EGFPCre} mice (Fig. 1b–e). Expression of IFN-γ in splenic $CD4^+$ T cells was markedly decreased in *Foxp3*^{EGFPCre}*Pofut1*$^{Δ/Δ}$ as compared to *Foxp3*^{EGFPCre} mice, whereas expression of IL-17 was unaffected (Fig. 1f, g). Similar results were obtained for the IFN-γ production by $CD8^+$ T cells (Fig. 1h, i). Expression of several T_{reg} cell markers, including Foxp3, CD25, CTLA-4, Helios and neuropilin 1 (Nrp1) was increased in Pofut1-deficient compared to

Foxp3^{EGFPCre} T_{reg} cells (Fig. 1j). We examined the role of the canonical Notch signaling in T_{reg} cells by lineage-specific deletion of *lox*P-flanked *Rbpj* (*Foxp3*^{EGFPCre}*Rbpj*$^{\Delta/\Delta}$; Supplementary Fig. 1a, b) [27]. The key phenotypes of *Foxp3*^{EGFPCre}*Pofut1*$^{\Delta/\Delta}$ mice were recapitulated in *Foxp3*^{EGFPCre}*Rbpj*$^{\Delta/\Delta}$ mice (Fig. 1a–j), indicating that the canonical pathway is the primary mediator of Notch signaling in T_{reg} cells. Of the four Notch receptors, Notch1 was the most highly expressed in T_{reg} cells, followed by Notch 2, whereas Notch3 and Notch4 expression was negligible (Supplementary Fig. 1c, d). The phenotype of mice with Notch1- deficient T_{reg} cells, achieved by lineage-specific deletion of *lox*P-flanked *Notch1* (*Foxp3*^{EGFPCre}*Notch1*$^{\Delta/\Delta}$; Supplementary Fig. 1a, b), approximated those of mice with Pofut- or RBPJ-deficient T_{reg} cells, indicating that Notch1 was the main receptor through which Notch signaling was triggered in T_{reg} cells (Fig. 1a–j) [28].

We also assessed the effect of loss of function mutations in genes encoding members of the Notch pathway on the generation of thymus-derived T_{reg} cells. We observed similar frequencies and numbers of Foxp3$^+$ T_{reg} cells among the mature CD4 single positive (CD4SP) thymocyte compartment in *Foxp3*^{EGFPCre}, *Foxp3*^{EGFPCre}*Pofut1*$^{\Delta/\Delta}$ *Foxp3*^{EGFPCre}*Rbpj*$^{\Delta/\Delta}$ and *Foxp3*^{EGFPCre}*Notch1*$^{\Delta/\Delta}$ mice (Supplementary Fig. 2a, b) we employed *Foxp3*^{YFPCre} mice, which express a fusion of yellow fluorescent protein (YFP) and Cre recombinase in Treg cells under control of the endogenous *Foxp3* locus [29]. We found that the *in vitro* differentiation of naive CD4$^+$ T cells from *Foxp3*^{YFPCre}*Rbpj*$^{\Delta/\Delta}$ or *Foxp3*^{EGFPCre}*Notch1*$^{\Delta/\Delta}$ into induced T_{reg} (iT_{reg}) cells was similar to that of *Foxp3*^{YFPCre} control cells (Supplementary Fig. 2c, d). These results indicate normal thymic development and peripheral differentiation of T_{reg} cell populations.

To further elucidate the cell-intrinsic impact of loss of function Notch mutations on T_{reg} cells, we took advantage of random X chromosome inactivation in females to analyze both central thymic and peripheral splenic T_{reg} cells in heterozygous *Foxp3*$^{YFPCre/+}$*Rbpj*$^{\Delta/\Delta}$ female mice. Compared to heterozygote *Foxp3*$^{YFPcre/+}$ littermate control female mice, in which approximately 50% of T_{reg} cells within the thymus and spleen are YFP$^+$, a higher proportion of YFP$^+$ T_{reg} cells was observed in the periphery of *Foxp3*$^{YFPCre/+}$*Rbpj*$^{\Delta/\Delta}$ females (Supplementary Fig. 2e, f). YFP$^+$ T_{reg} cells had higher expression of several T_{reg} cell markers, including CD25, Helios and Nrp1 compared to YFP$^-$ T_{reg} cells (Supplementary Fig. 2g, h). Overall, loss of function Notch signaling mutations exerted a positive, cell intrinsic effect on T_{reg} cell fitness and function both at steady state and in the context of inflammation.

T_{reg} cell-specific loss of Notch function protects mice from GVHD

We examined the suppressive capacities of Notch signaling-deficient T_{reg} cells in the context of a strong inflammatory response, using the model of major histocompatibility complex (MHC) class I&II disparate graft versus host disease (GVHD). Adoptive transfer of T cell-depleted bone marrow from *Foxp3*^{EGFPCre}, *Foxp3*^{EGFPCre}*Rbpj*$^{\Delta/\Delta}$ or *Foxp3*^{EGFPCre}*Notch1*$^{\Delta/\Delta}$ C57Bl/6 mice into BALB/c mice lead to recovery from the lethal irradiation (Fig. 2a). Co-transfer of total spleen cells from *Foxp3*^{EGFPCre} mice induced lethal GVHD, associated with expansion of donor-derived (H-2Kb$^+$) IFN-γ-producing CD4$^+$ and CD8$^+$ T cells (Fig. 2a–f), while co-transfer of *Foxp3*^{EGFPCre}*Rbpj*$^{\Delta/\Delta}$ or

Foxp3^{EGFPCre}*Notch1*$^{\Delta/\Delta}$ total spleen cells resulted in protection from lethal GVHD in recipient mice, with attenuated GVHD severity scores and decreased IFN-γ production by donor T cells (Fig. 2a–f). Moreover, transfer of total spleen cells from *Foxp3*^{EGFPCre}*RBPJ*$^{\Delta/\Delta}$ or *Foxp3*^{EGFPCre}*Notch1*$^{\Delta/\Delta}$ mice lead to increased frequency and number of donor T_{reg} cells, associated with decreased apoptosis, as assessed by Annexin V (AnnV) staining, and decreased IFN-γ production (Fig. 2c–d, g–j). In the context of exaggerated inflammation induced by GVHD, donor *Foxp3*^{EGFPCre} T_{reg} cells exhibited higher expression of the cleaved intracellular domain of Notch1 (N1c), as compared to their CD4$^+$Foxp3$^-$ T_{conv} cell counterparts (Fig. 2h–i) Together, these results reveal a direct role for cell-intrinsic Notch signaling in destabilizing T_{reg} cells in the context of inflammation by promoting their apoptosis and IFN-γ production.

T_{reg} cell-specific gain of Notch function disrupts peripheral tolerance

To investigate the role of Notch1 signaling in T_{reg} cells, we generated *Foxp3*^{EGFPCre}*Rosa26*$^{N1/N1c}$ mice, which constitutively express N1c in their T_{reg} cells (Supplementary Fig. 1e) [30]. We found increased expression of N1c in *Foxp3*^{EGFPCre}*Rosa26*$^{N1/N1c}$ T_{reg} cells, associated with heightened expression of several Notch signaling target genes, including *Hes1*, *Hey1*, *Heyl* and *Dtx1* (Supplementary Fig. 1f, g). In contrast to the mutations that resulted in loss of Notch function, constitutive expression of N1c in T_{reg} cells resulted in an autoimmune lymphoproliferative disease, whose manifestations included large vessel vasculitis and lymphocytic end organ infiltration in the *Foxp3*^{EGFPCre}*Rosa26*$^{N1/N1c}$ mice (Fig. 3a, b). The CD4$^+$CD62L^{lo}CD44^{hi} T effector memory cell pool was expanded and the numbers of CD4$^+$ and CD8$^+$ T cells expressing IFN-γ were increased by 50%, while the frequency of T_{reg} cells was decreased by 45% (Fig. 3c, d). There was also dysregulation of the B cell compartment with significant increase of several circulating autoantibodies (to 18 out of 98 screened endogenous antigens) in *Foxp3*^{EGFPCre}*Rosa26*$^{N1/N1c}$ mice as compared to *Foxp3*^{EGFPCre} mice (Fig. 3e). Overexpression of N1c in T_{reg} cells dramatically worsened the incidence and severity of type I diabetes in the genetically susceptible NOD mice, particularly in normally resistant NOD males (Fig. 3f–h). Whereas N1c expression in T cell precursors precipitates the occurrence of T cell acute lymphocytic leukemia, no evidence of leukemia was found in Foxp3^{EGFPCre}*Rosa26*$^{N1c/N1c}$ mice up to 6 months of age (data not shown) [4].

Analysis of *Foxp3*^{EGFPCre}*Rosa26*$^{N1c/N1c}$ mice revealed an age-dependent increase in the frequency of T_{reg} cells that do not express the *Foxp3* BAC-driven EGFP-Cre transgene (data not shown). Accumulation of EGFP$^-$ T_{reg} cells was observed during thymic development and reached up to 30% of the peripheral T_{reg} cell pool at 2 month of age (Supplementary Fig. 3a, b). EGFP$^-$ T_{reg} cells were observed at very low frequencies in Foxp3^{EGFPCre}, *Pofut1*, *RBPJ* or *Notch1* mice (**data not shown**). Whereas the GFP$^+$ Foxp3^{EGFPCre}*Rosa26*$^{N1c/N1c}$ T_{reg} cells expressed high amounts of N1c, consistent with the expression of the transgene from the *Rosa26* locus, N1c expression in GFP$^-$ *Foxp3*^{EGFPCre}*Rosa26*$^{N1c/N1c}$ T_{reg} cells was similar to that of control *Foxp3*^{EGFPcre} T_{reg} cells (Supplementary Fig. 3c), suggesting that the GFP$^-$ T_{reg} cells never expressed the *Foxp3*^{EGFPcre} BAC gene and that transgenic expression of N1c induced a profound competitive disadvantage in T_{reg} cells. To overcome this 'escape' phenotype, we used

Foxp3^{YFPCre} mice that expressed a YFP-Cre fusion protein under control of the endogenous *Foxp3* locus [29]. Unlike *Foxp3*^{EGFPCre}*Rosa26*$^{N1c/N1c}$ mice, 95% of Foxp3^{YFPCre}*Rosa26*$^{N1c/N1c}$ T_{reg} cells expressed the *Foxp3*-driven Cre recombinase (Supplementary Fig. 3d, e). Analysis of heterozygous *Foxp3*$^{YFPCre/WT}$*Rosa26*$^{N1c/N1c}$ females revealed marked skewing of X-chromosome utilization by T_{reg} cells in the periphery in favor of expressing the *Foxp3*^{WT} allele (Supplementary Fig. 3f, g). YFP^{+} *Foxp3*$^{YFPCre/WT}$*Rosa26*$^{N1c/N1c}$ T_{reg} cells expressed significantly lower amounts of Foxp3 compared to their YFP^{-} T_{reg} cell counterparts (Supplementary Fig. 3h, i). Double mutant *Foxp3*^{YFPCre}*Rosa26*$^{N1c/N1c}$ male mice developed a more aggressive and accelerated autoimmune lymphoproliferative disease than *Foxp3*^{EGFPCre}*Rosa26*$^{N1c/N1c}$ males, as revealed by tissue histology and immunological analyses (Supplementary Fig. 4). Altogether, these data indicate a profoundly deleterious impact of N1c expression on T_{reg} cell fitness.

Flow cytometric analysis of peripheral T_{reg} cells in the *Foxp3*^{EGFPCre}*Rosa26*$^{N1c/N1c}$ and *Foxp3*^{YFPCre}*Rosa26*$^{N1c/N1c}$ mice revealed decreased expression of T_{reg} cell markers, including Foxp3, CD25, CTLA-4, OX40, Helios, Nrp1 and Eos (Fig. 4a and Supplementary Fig. 5a, b). *Foxp3*^{EGFPCre}*Rosa26*$^{N1c/N1c}$ T_{reg} cells exhibited increased Ki67 expression, consistent with heightened cellular proliferation, and increased apoptosis, as detected by AnnV staining, as compared to *Foxp3*^{EGFPCre} and *Foxp3*^{EGFPCre}*Rbpj*$^{\Delta/\Delta}$ T_{reg} cells (Fig. 4b, c). *In vitro*, the suppressive capacity of *Foxp3*^{EGFPCre}*Rosa26*$^{N1c/N1c}$ T_{reg} cells was decreased, whereas that of *Foxp3*^{EGFPCre}*Rbpj*$^{\Delta/\Delta}$ T_{reg} cells was enhanced compared to *Foxp3*^{EGFPCre} T_{reg} cells (Fig. 4d). The generation of thymic T_{reg} cells in *Foxp3*^{EGFPCre}*Rosa26*$^{N1c/N1c}$ mice proceeded unaffected as similar frequencies and numbers of Foxp3^{+} cells among CD4 single positive thymocytes were found in *Foxp3*^{EGFPCre} and *Foxp3*^{EGFPCre}*Rosa26*$^{N1c/N1c}$ mice (Supplementary Fig. 5c–d). In addition, the demethylation status of the conserved non-coding sequence 2 (CNS2) CpG elements in the *Foxp3* promoter was similar in thymic T_{reg} cells of *Foxp3*^{EGFPCre} and *Foxp3*^{EGFPCre}*Rosa26*$^{N1c/N1c}$ mice. (Supplementary Fig. 5e–f). *In vitro*, the differentiation of naive CD4^{+} *Foxp3*^{YFPCre}*Rosa26*$^{N1c/N1c}$ T cells into induced T_{reg} (iT_{reg}) cells following stimulation with anti-CD3+CD28 mAb and TGF-β was decreased compared to those of *Foxp3*^{YFPCre} mice (Supplementary Fig. 5g, h), suggesting an inhibitory function of N1c in both thymus and periphery-derived T_{reg} cells. Next, we investigated the effect of N1c on the ability of adoptively transferred T_{reg} cells to suppress colitis in Rag1-deficient mice. Naive CD45Rb^{hi}CD4^{+} T_{conv} cells were isolated from CD45.1^{+} *Foxp3*^{EGFPCre} donor mice and transferred alone or in combination with Treg cells from CD45.2^{+} *Foxp3*^{EGFPcre} or CD45.2^{+} *Foxp3*^{EGFPcre}*Rosa26*$^{N1c/N1c}$ mice into T cell–deficient Rag1$^{-/-}$ host mice. We found that such co-transfer of Treg cells from CD45.2^{+} *Foxp3*^{EGFPcre}*Rosa26*$^{N1c/N1c}$ mice failed to suppress the colitis induced by the transfer of naive CD45.1^{+} CD45Rb^{hi}CD4^{+} T_{conv} cells: the recipient *Rag1*$^{-/-}$ mice exhibited substantial weight loss and tissue inflammation, as well as shorter colons and excess generation of IFN-γ^{+} and IL-17^{+} CD45.1^{+} effector T cells (Fig. 4e–i). Analysis of the CD45.2 cell compartment in recipient mice at d35 showed increased EGFP loss in *Foxp3*^{EGFPCre}*Rosa26*$^{N1c/N1c}$ (60%) as compared to control *Foxp3*^{EGFPCre} cells (45%) (Fig. 4j), indicative of the heightened instability of N1c-expressing T_{reg} cells.

To delineate the intrinsic impact of N1c on the functional phenotype of T_{reg} cells, as opposed to a cell-extrinsic effect mediated by systemic inflammation, we analyzed heterozygous *Foxp3*$^{YFPCre/WT}$*Rosa26*$^{N1c/N1c}$ female mice for lymphoproliferation, immune cell activation and T_{reg} cell phenotype. In contrast to homozygous *Foxp3*$^{YFPCre/YFPCre}$*Rosa26*$^{N1c/N1c}$ females, *Foxp3*$^{YFPCre/WT}$*Rosa26*$^{N1c/N1c}$ females exhibited no signs of lymphoproliferation or T_H1 skewing of $CD4^+$ T_{conv} cells at steady state (Supplementary Fig. 6a–d). However, YFP^+ T_{reg} cells from Foxp3$^{YFPCre/WT}$*Rosa26*$^{N1c/N1c}$ females showed decreased expression of T_{reg} cell markers such as Foxp3, CD25, CTLA4, OX40, Helios and Nrp1, as compared to YFP^- T_{reg} cells from the same mice (Supplementary Fig. 6e, f). These results indicate that N1c overexpression destabilizes the phenotype and impairs the function of T_{reg} cells by a cell-intrinsic mechanism, leading to immune cell activation, lymphoproliferation and autoimmunity.

The canonical Notch pathway mediates T_{reg} cell destabilization

To determine the overall contribution of the canonical Notch pathway to the inflammation and autoimmunity observed in *Foxp3*^{EGFPCre}*Rosa26*$^{N1c/N1c}$ mice, we concurrently deleted *Rbpj* in the T_{reg} cells of these mice. Most major phenotypes of *Foxp3*^{EGFPCre}*Rosa26*$^{N1c/N1c}$ mice, including lymphoproliferation, T cell activation, T_H1 and T^C1 skewing, autoantibody production and alterations in T_{reg} cell markers and suppressor function were reversed in *Foxp3*^{EGFPCre}*Rosa26*$^{Nc1/N1c}$*Rbpj*$^{\Delta/\Delta}$ mice (Fig. 5a–i). Thus, activation of canonical Notch signaling has a predominant role in the immune dysregulation observed in the *Foxp3*^{EGFPCre}*Rosa26*$^{N1c/N1c}$ mice.

Notch activates RBPJ-dependent and independent transcription in T_{reg} cells

T_{reg} cells have a transcriptional signature reflective of their regulatory function [31, 32, 33]. We compared the transcriptional profiles of splenic T_{reg} cells isolated from *Foxp3*^{EGFPCre}, *Foxp3*^{EGFPCre}*Rosa26*$^{N1c/N1c}$, *Foxp3*^{EGFPCre}*Rbpj*$^{\Delta/\Delta}$ and *Foxp3*^{EGFPCre}*Rosa26*$^{N1c/N1c}$*Rbpj*$^{\Delta/\Delta}$ mice. We compared the transcriptional profiles of splenic Treg cells isolated from *Foxp3*^{EGFPCre}, *Foxp3*^{EGFPCre}*Rosa26*$^{N1c/N1c}$, *Foxp3*^{EGFPCre}*Rbpj*$^{\Delta/\Delta}$ and *Foxp3*^{EGFPCre}*Rosa26*$^{N1c/N1c}$*Rbpj*$^{\Delta/\Delta}$ mice. Comparison of the transcriptional profiles of *Foxp3*^{EGFPCre}*Rosa26*$^{N1c/N1c}$ T_{reg} cells and *Foxp3*^{EGFPCre} T_{reg} cells revealed a limited set of genes whose transcription was affected by N1c expression (mean expression value, >120; false-discovery rate, <0.1; coefficient variation, <0.5; Fig. 6a). Plotting of the transcriptional profiles as the difference in expression in *Foxp3*^{EGFPCre}*Rosa26*$^{N1c/N1c}$ T_{reg} cells versus $_{Foxp3}^{EGFPCre}$ T_{reg} cells against the difference in expression *Foxp3*^{EGFPCre}*Rosa26*$^{N1c/N1c}$ $_{Rbpj}^{\Delta/\Delta}$ T_{reg} cells versus $_{Foxp3}^{EGFPCre}$ T_{reg} cells revealed both RBPJ-dependent alterations in gene expression and RBPJ-independent alterations in gene expression (Fig. 6b). Hierarchal clustering analysis of genes whose expression was significantly altered by N1c expression revealed a subgroup of genes that were either upregulated (*Dtx1, Ifng, Gzmb, Pde3b*) or down-regulated (*Nrp1, Socs2, Il1rl1, Ikzf2, Ikzf4*) in an RBPJ-dependent manner (Fig. 6c). A second subgroup included genes that were modulated by N1c in an RBPJ-independent manner, consistent with their regulation by non-canonical pathway(s) (Fig. 6d). This subgroup included genes downstream of Foxo1 signaling, such as *Bmp7, Gzma, Cd55* and others [34, 35, 36]. These results indicated a

profound impact of Notch signaling on the T_{reg} cell transcriptome by both canonical and non-canonical pathways.

We further analyzed the binding of RBPJ at two Foxp3-regulated genes that were affected by N1c expression. These included *Pde3b*, whose expression is normally suppressed by Foxp3, but was upregulated by N1c expression in T_{reg} cells, and *Ikzf2*, whose expression is normally upregulated by Foxp3, but was decreased by N1c. Chromatin-immunoprecipitation analysis indicated that Foxp3 binding to the *Pde3b* and *Ikzf2* promoters was decreased, and that of RBPJ was increased, in *Foxp3*^{EGFPCre}*Rosa26*$^{N1c/N1c}$ as compared to *Foxp3*^{EGFPCre} T_{reg} cells (Supplementary Fig. 7a, b). Analysis of epigenetic histone-methylation markings at the $_{Pde3b}$ promoter revealed more H3K4me3 and less H3K27me2 in $_{Foxp3}^{EGFPCre}{}_{Rosa26}^{N1c/N1c}$ T_{reg} cells than in $_{Foxp3}^{EGFPCre}$ T_{reg} cells (Supplementary Fig. 7a), a pattern associated with decreased Foxp3-dependent suppression of gene expression[37]. Reciprocally, H3K27me2 was increased at the *Ikzf2* promoter (Supplementary Fig. 7b). These results indicate that canonical Notch signaling directly targeted a subset of Foxp3-regulated genes, antagonized Foxp3 binding and altered Foxp3-induced epigenetic markings at those loci.

The Notch canonical pathway mediates T_H1 reprograming of T_{reg} cells

Aborted T_H1 programming provides a mechanism by which T_{reg} cells restrain T_H1 responses [38]. T_{reg} cells respond to IFN-γ treatment by upregulating *Tbx21* expression in a STAT1-dependent manner [38]. T-bet expression in T_{reg} cells induces a partial Th1 program, including expression of CXCR3, but fails to upregulate expression of IL-12Rβ2, necessary to complete STAT4-dependent T_H1 differentiation [39]. N1c over-expression in *Foxp3*^{EGFPCre}*Rosa26*$^{N1c/N1c}$ T_{reg} cells upregulated the transcription of several genes associated with T_H1 cells, including *Il12rb2 and Ifng* as well as a number of genes downstream of IL-12-STAT4 signaling, including *Ffar1*, *Id2* and *Nkg7* (Fig. 7a and Supplementary Table 1). Treatment of *Foxp3*^{EGFPCre}*Rosa26*$^{N1c/N1c}$ T_{reg} cells with IL-12 lead to expression of IFN-γ, which was lost in *Foxp3*^{EGFPCre}*Rosa26*$^{N1c/N1c}$*Rbpj*$^{Δ/Δ}$ T_{reg} cells (Fig. 7b, c). Treatment with IL-12 resulted in the phosphorylation of STAT4 in a subset of N1c-expressing T_{reg} cells in an RBPJ-dependent manner (Fig. 7d, e). *Foxp3*^{EGFPCre}*Rosa26*$^{N1c/N1c}$ T_{reg} cells exhibited increased RBPJ and N1c binding to the *Ifng* CNS22 element, which mediates transcriptional activation of *Ifng* by Notch signaling in cooperation with T-bet (Fig. 7f, g) [40]. IL-12-induced STAT4 phosphorylation was only observed in YFP^+, but not YFP^- T_{reg} cells from heterozygous Foxp3$^{YFPcre/+}$*Rosa26*$^{N1c/N1c}$ females (Supplementary Fig. 6g, h), indicating that expression of *Il12rb2* in Foxp3$^{YFPcre/WT}$*Rosa26*$^{N1c/N1c}$ T_{reg} cells was due to intrinsic N1c-overexpressing and not to systemic inflammation. These results indicated that N1c promoted T_H1 programming of T_{reg} cells in a cell-intrinsic and canonical pathway-dependent manner.

Notch regulates *Foxp3* epigenetic stability via Rictor

Notch signaling activates the mammalian target of Rapamycin (mTOR) kinase complex 2 (mTORC2) and its downstream kinase AKT independent of RBPJ[3, 4, 41]. AKT phosphorylates the transcription factor Foxo1, resulting in its retention in the cytosol and its ubiquitinaiton and degradation[42, 43]. In turn, Foxo1 negatively regulates Th1 differentiation

of T_{reg} cells by suppressing *Ifng* transcription, as well as other type 1 genes [35, 44]. Because N1c overexpression increased the transcription of Foxo1- suppressed genes in *Foxp3*^{EGFPCre}*Rosa26*$^{N1c/N1c}$ T_{reg} cells, we examined mTORC2-Akt activation in these cells. Anti-CD3+CD28 mAb treatment resulted in increased phosphorylation of S473 in AKT, which is a target of mTORC2, in *Foxp3*^{EGFPCre}*Rosa26*$^{N1c/N1c}$ T_{reg} cells, but not in control *Foxp3*^{EGFPCre} T_{reg} cells. Anti-CD3 mAb treatment did not induce the phosphorylation of T308 in AKT, which is a target of phospho-inositide 3-kinase (PI3K) (Fig. 8a, b and **data not shown**). AKT S473 phosphorylation was detected in *Foxp3*^{EGFPCre}*Rosa26*$^{N1c/N1c}$*Rbpj*$^{\Delta/\Delta}$ T_{reg} cells as well, suggesting it was independent of RPBJ (Fig. 8a, b). AKT S473 phosphorylation was not observed in *Foxp3*^{EGFPCre}*Rosa26*$^{N1c/N1c}$*Rictor*$^{\Delta/\Delta}$ T_{reg} cells, bearing a Foxp3-driven deletion of Rictor, an essential component of the mTORC2 complex following anti- CD3+CD28 mAb stimulation (Supplementary Fig. 1a, b). In contrast, AKT S473 phosphorylation proceeded unaffected in stimulated $CD4^+$ T_{conv} cells of all genotypes (Fig. 8a, b). There was increased Foxo1 translocation to the cytosol upon CD3 activation in *Foxp3*^{EGFPCre}*Rosa26*$^{N1c/N1c}$ T_{reg} cells, which was partially reversed by Rictor but not by RBPJ deficiency in these cells (Fig. 8c, d).

Analysis of *Foxp3*^{EGFPCre}*Rosa26*$^{N1c/N1c}$*Rictor*$^{\Delta/\Delta}$ mice revealed that the frequencies and absolute numbers of splenic T_{reg} and IFN-γ^+CD4^+ T_{conv} cells were decreased and the lymphoproliferative disease was reduced as compared to Foxp3^{EGFPCre}*Rosa26*$^{N1c/N1c}$ mice, (Supplementary Fig. 8a,b). However, in the absence of N1c overexpression, Rictor deficiency did not impact the frequencies or the total numbers of IFN-γ^+ $CD4^+$ T cells, memory $CD4^+$ T cells or T_{reg} cells in *Foxp3*^{EGFPCre}*Rictor*$^{\Delta/\Delta}$ as compared to *Foxp3*^{EGFPCre} mice (Supplementary Fig. 8c, d). Importantly, the escape of *Foxp3*^{EGFPCre} *Rosa26*$^{N1c/N1c}$ T_{reg} cells away from expressing the *Foxp3*^{EGFPCre} BAC transgene was ameliorated by concurrent RBPJ but not Rictor deficiency, indicative of the failure of Rictor deficiency to correct the impaired fitness of N1c–expressing T_{reg} cells (Fig. 8e, f). However, expression of key T_{reg} cell markers was improved in *Foxp3*^{EGFPCre} *Rosa26*$^{N1c/N1c}$*Rictor*$^{\Delta/\Delta}$ as compared to *Foxp3*^{EGFPCre}*Rosa26*$^{N1c/N1c}$ T_{reg} cells (Supplementary Fig. 8e, f).

Epigenetic demethylation of the *Foxp3* CNS2 region has been linked to sustained Foxp3 expression and overall Treg cell stability [45, 46]. The demethylation of the *Foxp3* CNS2 region was decreased in *Foxp3*^{EGFPCre}*Rosa26*$^{N1c/N1c}$ as compared to *Foxp3*^{EGFPCre} T_{reg} cells, which was largely reversed by concurrent Rictor but not RBPJ deficiency (Fig. 8g, h). These findings indicated that N1c destabilized T_{reg} cells in part by altering their *Foxp3* CNS2 epigenetic demethylation signature in a Rictor-dependent manner.

Discussion

In this study, we provide evidence that cell-intrinsic Notch signaling regulates the T_{reg} cell compartment in the periphery and controls T_{reg} cell programming towards a T_H1 phenotype, as well as T_H1 cell responses. Blockade of different steps of the Notch signaling pathway in T_{reg} cells, by means of lineage-specific targeted gene inactivation of *Pofut1*, *Rbpj* or *Notch1*, resulted in increased T_{reg} cell frequency, decreased $CD4^+$ T cell compartment size, and decreased IFN-γ production by CD4 and CD8 cells. T_{reg} cell-specific deletion of Notch

signaling components protected against full MHC-mismatched GVHD in association with decreased T_{reg} cell apoptosis, T_{reg} cell programing towards a T_H1 phenotype and alloreactive T_H1 and T_C1 responses. Reciprocally, over-expression of N1c in T_{reg} cells resulted in lymphoproliferation, increased T_{reg} cell apoptosis, T_H1 programing of T_{reg} cells, dysregulated T_H1 and T_C1 responses and autoimmunity. N1c expression down-regulated the expression of several critical components of the T_{reg} cell transcriptome and weakened the T_{reg} cell epigenetic imprint. Thus, homeostatic Notch signaling in T_{reg} cells defines the size and function of the T_{reg} cell compartment and controls the magnitude of T_H1 and T_C1 cell responses *in vivo*.

The effects of Notch signaling on T_{reg} cells were predominantly exerted by the canonical pathway. Interruption of the canonical Notch pathway by means of T_{reg} cell-specific *Rbpj* deletion rescued the key manifestations associated with enforced N1c expression in T_{reg} cells, including lymphoproliferation and autoimmunity. Several T_{reg} cell phenotypic, transcriptional and functional alterations induced by enforced N1c expression were reversed upon RBPJ deletion, indicating their dependence on canonical Notch signaling. RBPJ bound to a subset of Foxp3 target gene, such as *Pde3b* and *Ikzf2*, antagonized the binding of Foxp3 and reversed the Foxp3-associated histone methylation profile at those loci, indicative of a direct effect of the canonical pathway on at least a subset of Foxp3-regulated genes. Additional regulation may also be exerted by downstream gene targets of Notch signaling, such as *Hes1* and *Dtx1*, which may engage in secondary transcriptional circuits that contribute to gene expression changes induced by Notch in T_{reg} cells.

In contrast to the above, a number of T_{reg} cell transcripts appeared to respond to Notch signaling in a canonical pathway-independent manner. Several of these have been previously associated with Foxo1 dependent regulation, consistent with their induction by the mTOR-AKT-Foxo1 pathway. N1c-driven impairment of epigenetic demethylation of *Foxp3* CNS2 was also independent of the canonical pathway, suggesting a putative role for non-canonical signaling in Notch-mediated T_{reg} cell destabilization. This conclusion was reinforced by the demonstration that N1c-induced increase in CpG methylation of *Foxp3* CNS2 was largely reversed in N1c overexpressing but Rictor deficient T_{reg} cells

These studies highlight the important role played by canonical Notch signaling in T_{reg} cells in enabling T_H1 and T_C1 responses. In the course of controlling a T_H1 response, T_{reg} cells normally undergo an aborted program of T_H1 differentiation that limits their capacity to express IL-12Rβ2 [38]. Activation of the canonical Notch signaling bypassed this blockade, leading to STAT4 activation and IFN-γ production in response to IL-12 in T_{reg} cells. RBPJ and N1c associated with CNS22 in the *Ifng* locus in N1c-overexpressing T_{reg} cells, consistent with previous data showing direct activation of *Ifng* expression by Notch signaling in synergy with T-bet [40]. N1c also enabled more effective activation of mTORC2-AKT by TCR engagement and Foxo1 cytosolic sequestration, a mechanism previously implicated (by means of $CD4^+$ T cell- or T_{reg} cell-specific *Foxo1* deletion) in promoting T_H1 differentiation of T_{reg} cells [34, 35, 44]. The two mechanisms, canonical and non-canonical, may thus act cooperatively to induce T_H1 skewing.

Notch signaling in T_{reg} cells played a particularly deleterious role in the context of severe inflammation in the full MHC-mismatched GVHD. Whereas control (*Foxp3*^{EGFPCre}) T_{reg} cells were susceptible to apoptosis and T_H1 programming, Notch1 or RBPJ-deficient T_{reg} cells were resistant to both processes, leading to the accumulation of T_{reg} cells, decreased skewing towards the T_H1 phenotype and increased survival. Notch1 inactivation in T cells protects against GVHD[22], and our studies indicated that T_{reg} cells were the key cellular effectors of this effect. In the context of overwhelming T_H1 immune responses, such as experimental *T. gondii* infection, T_{reg} cells undergo T_H1 programming and apoptosis, recapitulating the fate of T_{reg} cells in GVHD [47]. The exaggerated T_H1 response in *T. gondii*-infected mice was associated with decreased IL- 2 production, which contributed to T_{reg} cell apoptosis. In addition, interference with Notch signaling in T_{reg} cells attenuated the T_H1 and T_C1 response and increased IL-2 production, consistent with a role for IL-2 in enhanced survival of Notch-deficient T_{reg} cells in GVHD.

The inhibitory effects of Notch signaling on T_{reg} cell function offer mechanistic insights into how blockade of Notch receptors may induce tolerance, as has been reported in some experimental mouse models of graft versus host disease. Intervention strategies targeting the Notch pathway may thus offer innovative therapeutic approaches in transplant and autoimmune diseases.

Online Methods

Mice

Foxp3^{EGFPCre}, *Foxp3*^{YFPCre}, *Notch1*$^{fl/fl}$, *Rosa26*$^{N1c/N1c}$, *Rag1*$^{-/-}$, CD45.1, *Foxp3*^{EGFP} and BALB/c mice were obtained from the Jackson Laboratory [28, 30, 48]. *Rictor*$^{fl/fl}$ mice were obtained from the Mutant Mouse Regional Resource Center. *Pofut1*$^{fl/fl}$ and *Rbpj*$^{fl/fl}$ were kind gifts of Pamela Stanley and Tasuku Honjo, respectively, and were generated as described [26, 27]. All Foxp3 mutant mouse strains and their respective crosses were backcrossed 8–10 generations on C57BL/6 or NOD background where specified. Excepted when it was specified, 8 weeks old mice were used in this study. The mice were housed under specific pathogen-free conditions and used according to the guidelines of the institutional Animal Research Committees at the Boston Children's Hospital.

Real-time PCR

Total RNA was isolated from sorted cells with RNeasy kit (Qiagen). Reverse transcription was performed with the SuperScript III RT-PCR system (Invitrogen) and quantitative real-time reverse transcription (RT)-PCR with Taqman® Fast Universal PCR master mix, internal house keeping gene mouse (GAPD VIC-MGB dye) and specific target gene primers (FAM Dye) (Applied Biosystems) on Step-One- Plus machine. Relative expression was normalized to GAPD for Notch1-4 receptor and calculated as fold change compared to wild-type $CD4^+GFP^-$ conventional T cells for *Pofut1*, *Notch1*, *RBPJ* and *Rictor* regarding the regulatory T cell-specific deficiency and fold change normalized to wild-type Treg cells for *IFNg* and *IL12rb2*.

Flow cytometry

Annexin V and antibodies against CD4, CD8, CD16/CD32, CD90.2, CTLA4, ICOS, H-2K^{d} (biolegend), CD3Σ, CD25, CD44, CD45.1, CD45.2, CD45Rb, CD62L, Eos, Foxp3, Helios, IFN-γ, IL-17A, IL-2, Ki67, OX40, CXCR3, H-2K^{b} (eBioscience), N1c, P-STAT4 (BD biosciences), P-AKT (S473) (Cell signaling) and Nrp1 (R&D system) were used. Cell suspensions were incubated for 10 min with CD16/CD32 then stained for surface markers for 20 min on PBS/1%FCS. Foxp3, Helios, Eos, CTLA4, Ki67 staining was performed by using eBioscience Fixation/Permeabilization kit. For cytokine detection, cell suspensions were pre-incubated with 50 ng/mL PMA, 500 ng/mL ionomycin and 10 μg/mL brefeldin A for 4h in complete medium before CD16/32 blocking followed by surface staining, permeabilization and intracellular Foxp3, IFN-γ, IL-2 and IL-17 staining. For phospho-AKT experiments, spleen cells were stimulated for 30 min with soluble anti-CD3 (1μg/mL) and anti-CD28 (5μg/mL). In some experiments, spleen cells were pre-treated with Rapamycin (250nM, Tocris) for 0, 1 or 24h. After stimulation, cells are fixed with PBS/2%PFA for 20min, permeabilized in 90% methanol for 30 min on ice and stained for CD4, Foxp3 and P^{S473}-AKT. For phospho-STAT4 experiments, splenic CD4^{+} T cells were isolated and stimulated for 30min with 25ng/mL of recombinant mouse IL-12 (Biolegend). Cells were fixed with PBS/2%PFA for 20min, permeabilized in 90% methanol for 30 min on ice and stained for CXCR3, CD4, Foxp3 and P^{Y693}-STAT4. For *ex-vivo* Treg cell stimulation, isolated Treg cells were cultured for 3 days with IL-2 at 200U/mL ± IL-12 at 25 ng/mL (Biolegend) and PMA/ionomycin/BrefeldinA the last 4 hours before staining for IFN-γ and Foxp3. All flow cytometry acquisitions were performed on a Fortessa cytometer using DIVA software (BD Biosystems) and analyzed using FlowJo (Tree Star).

Graft versus host disease

Eight weeks old Balb/c mice were lethally irradiated (8.5–9 Gy) 4 hours prior reconstitution with 5.10^{6} T cell depleted bone marrow cells alone or in presence of 10^{7} spleen cells from C57BL/6 *Foxp3*^{EGFPCre}, *Foxp3*^{EGFPCre}*Rbpj*$^{Δ/Δ}$ or *Foxp3*^{EGFPCre}*Notch1*$^{Δ/Δ}$ mice. T cell deplete bone marrow was prepared using CD90.2 microbeads (Miltenyi Biotech). Clinical GVHD score was evaluated every 2 to 3 days by assessment of five clinical parameters as followed: Weight loss (<10%, grade 0; >10% to <20%, grade 1; >20%, grade 2), posture (Normal, grade 0; Hunching noted only at rest, grade 1; Severe hunching and/or impairs movement, grade 2), activity (Normal, grade 0; Mild to moderately decreased, grade 1; Stationary unless stimulated, grade 2), fur texture (Normal, grade 0; Mild to moderate ruffling, grade 1; Severe ruffling/poor grooming, grade 2) and skin integrity (Normal, grade 0; Scaling of paws/tail, grade1; Obvious areas of denuded skin, grade 2). In selected experiments, mice were sacrificed 5 days post transplantation and donor H-2Kd^{-}H-2Kb^{+} T cells were evaluated for apoptosis, cytokine production and Foxp3 expression.

Adoptive transfer induced Colitis

Naïve (CD4^{+}CD45RB^{high}GFP^{-}) and T$_{reg}$ (CD4^{+}GFP^{+}) cells are respectively isolated from the spleen of CD45.1 and CD45.2 *Foxp3*^{EGFPCre} or *Foxp3*^{EGFPCre}*Rosa26*$^{N1c/N1c}$ mice. Colitis was induced in RAG1-deficient males by i.p. injection of 5.10^{5} CD45.1 naive ± 2.10^{5} T$_{reg}$ cells. Mice were weighed and monitored for signs of disease twice weekly.

Suppression assays

$CD4^+$ T cells were isolated using a CD4 negative isolation kit (Miltenyi), then labeled with CellTrace™ Violet Cell Proliferation dye (Life technologies) according to the manufacturer's instructions and used as responder cells. Treg ($CD4^+GFP^+$) cells were isolated on FACSAria and used as suppressor cells. Responders were used at a fixed concentration of 10^5 cells per well and stimulated for 3 days with 2 μg/mL of soluble anti-CD3 antibody and 5 μg/mL of soluble anti-CD28 antibody in the presence of 4.10^5 feeder *Rag1*$^{-/-}$ spleen cells in 96-well, round-bottom plates in triplicate.

Gene-expression profiling

Spleen T_{reg} ($CD3^+CD4^+GFP^+$) cells were double-sorted from 6 week old male *Foxp3*^{EGFPCre}, *Foxp3*^{EGFPcre}*Rbpj*$^{\Delta/\Delta}$, Foxp3^{EGFPcre}*Rosa26*$^{N1c/N1c}$ and *Foxp3*^{EGFPcre}*Rosa26*$^{N1c/N1c}$*Rbpj*$^{\Delta/\Delta}$ mice (n=3–4 per group). Cells were collected directly into TRIzol. RNA was purified and used for probe synthesis for hybridization to Affymetrix Mouse Gene M1.0 ST microarrays. Raw data were background-corrected and normalized with the RMA algorithm in the GenePattern software package [49].

ChIP assays

Chromatin immunoprecipitation on purified T_{reg} cells was performed with Agarose ChIP Kit (Pierce) and anti-RBPJ (Cell signaling), anti-Notch1 (biolegend), anti- Foxp3 (MBL), anti-Histone H3 trimethylated on Lysine 4 (H3K4me3) (abcam), anti-dimethylated on Lysine 27 (H3K27me2) (Millipore) and respective isotype control antibodies. Purified DNA was subjected to real-time PCR with primers flanking RBPJ binding site at *Ifng CNS-22* or with primers flanking Foxp3 binding sites on *Pde3b* and *Ikzf2* as previously described [40 37].

Histology

Pancreatic inflammation was scored based on the degree of inflammatory cellular infiltrations present in the islets of Langerhans: 0, no inflammation; 1, mild inflammatory infiltrates; 2, periinsulitis; 3, moderate and diffuse or severe and focal insulitis; 4, severe and diffuse insulitis; 5, severe insulitis and destruction of the tissue. For colitis experiments, colon sections were stained by H&E and scored as followed: 0, no inflammation; 1, mild, scattered infiltrates; 2, moderate infiltrates without loss of epithelium integrity; 3, moderate and diffuse or severe inflammation; 4, Severe inflammation associated with loss of the epithelial barrier integrity.

Autoantibody arrays

Screening for a broad panel of IgG autoantibodies was performed with autoantibody arrays (University of Texas Southwestern Medical Center, Genomic and Microarray Core Facility) as described [50].

Methylation analysis

The methylation status of *Foxp3* T_{reg}-specific demethylation region (TSDR or CNS2) in thymic and splenic Treg cells of 8 weeks old male mice was assessed by bisulfite sequence analysis, as described [51]. The TSDR of converted DNA was amplified by methylation-

specific primer sequences: *Foxp3 CNS2* Forward 5′-TATTTTTTTGGGTTTTGGGATATTA-3′ (forward) and *Foxp3 CNS2* Reverse 5′-AACCAACCAACTTCCTACACTATCTAT-3′. The PCR product was subcloned and sequenced [51]. Blast analyses were done by comparing the resulting sequences with converted *Foxp3* gene sequences.

Confocal microscopy

T_{reg} cells were purified and incubated on pre-coated coverslip (poly-L-lysin 50μg/mL, ± anti-CD3 0.1 or 1 μg/mL for low and high dose respectively) at 37°C for 30 min in RPMI/10%FCS. After fixation with PBS/4% paraformaldehyde, cells were permeabilized with PBS/0.1% saponin and blocked on PBS/4% bovine serum albumin (BSA). Cells were incubated with 1:100 diluted rabbit anti-Foxo1 (C29H4, Cell Signaling) followed by 1:500 diluted Alexa fluor 555-anti rabbit secondary antibody (Life technologies) in PBS/1%BSA. Slides were mounted with gold anti-fade reagent with DAPI (Invitrogen). Images were acquired with a Zeiss LSM700 confocal microscopy and ZEN imaging software. Five to 10 fields were selected randomly and total cells in the field were analyzed for percentage of Foxo1 nuclear localization using ImageJ software. Percentage of nuclear Foxo1 localization was obtained by the formula: 100 × corrected nuclear fluorescence/corrected total cell fluorescence and corrected fluorescence was obtained by the formula: Integrated Density – (Area of selected cell or nucleus × Mean fluorescence of background).

In vitro induced T_{reg} cell generation

Naive $CD4^+CD62L^{hi}CD44^{lo}$ T cells were isolated from spleen using FACS Aria (purity>98%, data not shown). Cells are stimulated *in vitro* with coated anti-CD3 (2μg/mL) and anti-CD28 (5μg/mL) for 5 days in the presence of different concentrations of rhTGF-β1 (0, 1, 2 or 5 ng/mL) [52].

Statistical analysis

Data were analyzed by paired and unpaired two-tailed Student's *t*-test, one and two way ANOVA with post test analyses and log-rank test, as indicated. Differences in mean values were considered significant at a $p < 0.05$.

Supplementary Material

Refer to Web version on PubMed Central for supplementary material.

Acknowledgments

This work was supported by National Institutes of Health grants 2R01AI065617, 2R01AI085090 and 1R56AI115699-01 (to T.A.C.). We thank Christophe Benoist for critical reading of the manuscript, and Pamela Stanley and Tasuku Honjo for respectively providing us with *Pofut1*$^{fl/fl}$ and *Rbpj*$^{fl/fl}$ mice.

References

1. Yuan JS, Kousis PC, Suliman S, Visan I, Guidos CJ. Functions of notch signaling in the immune system: consensus and controversies. Annu Rev Immunol. 2010; 28:343–365. [PubMed: 20192807]

2. Radtke F, Fasnacht N, Macdonald HR. Notch signaling in the immune system. Immunity. 2010; 32(1):14–27. [PubMed: 20152168]

3. Perumalsamy LR, Marcel N, Kulkarni S, Radtke F, Sarin A. Distinct spatial and molecular features of notch pathway assembly in regulatory T cells. Sci Signal. 2012; 5(234):ra53. [PubMed: 22827997]

4. Lee K, Nam KT, Cho SH, Gudapati P, Hwang Y, Park DS, et al. Vital roles of mTOR complex 2 in Notch-driven thymocyte differentiation and leukemia. J Exp Med. 2012; 209(4):713–728. [PubMed: 22473959]

5. Elyaman W, Bassil R, Bradshaw EM, Orent W, Lahoud Y, Zhu B, et al. Notch receptors and Smad3 signaling cooperate in the induction of interleukin-9- producing T cells. Immunity. 2012; 36(4): 623–634. [PubMed: 22503540]

6. Osipo C, Golde TE, Osborne BA, Miele LA. Off the beaten pathway: the complex cross talk between Notch and NF-kappaB. Laboratory investigation; a journal of technical methods and pathology. 2008; 88(1):11–17.

7. Poellinger L, Lendahl U. Modulating Notch signaling by pathway-intrinsic and pathway-extrinsic mechanisms. Current opinion in genetics & development. 2008; 18(5):449–454. [PubMed: 18722525]

8. Amsen D, Antov A, Flavell RA. The different faces of Notch in T-helper-cell differentiation. Nat Rev Immunol. 2009; 9(2):116–124. [PubMed: 19165228]

9. Cho OH, Shin HM, Miele L, Golde TE, Fauq A, Minter LM, et al. Notch regulates cytolytic effector function in CD8+ T cells. J Immunol. 2009; 182(6):3380–3389. [PubMed: 19265115]

10. Maekawa Y, Minato Y, Ishifune C, Kurihara T, Kitamura A, Kojima H, et al. Notch2 integrates signaling by the transcription factors RBP-J and CREB1 to promote T cell cytotoxicity. Nat Immunol. 2008; 9(10):1140–1147. [PubMed: 18724371]

11. Maekawa Y, Tsukumo S, Chiba S, Hirai H, Hayashi Y, Okada H, et al. Delta1- Notch3 interactions bias the functional differentiation of activated CD4+ T cells. Immunity. 2003; 19(4):549–559. [PubMed: 14563319]

12. Minter LM, Turley DM, Das P, Shin HM, Joshi I, Lawlor RG, et al. Inhibitors of gamma-secretase block in vivo and in vitro T helper type 1 polarization by preventing Notch upregulation of Tbx21. Nat Immunol. 2005; 6(7):680–688. [PubMed: 15991363]

13. Amsen D, Antov A, Jankovic D, Sher A, Radtke F, Souabni A, et al. Direct regulation of Gata3 expression determines the T helper differentiation potential of Notch. Immunity. 2007; 27(1):89–99. [PubMed: 17658279]

14. Tu L, Fang TC, Artis D, Shestova O, Pross SE, Maillard I, et al. Notch signaling is an important regulator of type 2 immunity. J Exp Med. 2005; 202(8):1037–1042. [PubMed: 16230473]

15. Fang TC, Yashiro-Ohtani Y, Del Bianco C, Knoblock DM, Blacklow SC, Pear WS. Notch directly regulates Gata3 expression during T helper 2 cell differentiation. Immunity. 2007; 27(1):100–110. [PubMed: 17658278]

16. Amsen D, Blander JM, Lee GR, Tanigaki K, Honjo T, Flavell RA. Instruction of distinct CD4 T helper cell fates by different notch ligands on antigen-presenting cells. Cell. 2004; 117(4):515–526. [PubMed: 15137944]

17. Keerthivasan S, Suleiman R, Lawlor R, Roderick J, Bates T, Minter L, et al. Notch signaling regulates mouse and human Th17 differentiation. J Immunol. 2011; 187(2):692–701. [PubMed: 21685328]

18. Mukherjee S, Schaller MA, Neupane R, Kunkel SL, Lukacs NW. Regulation of T cell activation by Notch ligand, DLL4, promotes IL-17 production and Rorc activation. J Immunol. 2009; 182(12):7381–7388. [PubMed: 19494260]

19. Barbarulo A, Grazioli P, Campese AF, Bellavia D, Di Mario G, Pelullo M, et al. Notch3 and canonical NF-kappaB signaling pathways cooperatively regulate Foxp3 transcription. J Immunol. 2011; 186(11):6199–6206. [PubMed: 21508258]

20. Ou-Yang HF, Zhang HW, Wu CG, Zhang P, Zhang J, Li JC, et al. Notch signaling regulates the FOXP3 promoter through RBP-J- and Hes1-dependent mechanisms. Molecular and cellular biochemistry. 2009; 320(1–2):109–114. [PubMed: 18777163]

21. Samon JB, Champhekar A, Minter LM, Telfer JC, Miele L, Fauq A, et al. Notch1 and TGFbeta1 cooperatively regulate Foxp3 expression and the maintenance of peripheral regulatory T cells. Blood. 2008; 112(5):1813–1821. [PubMed: 18550850]
22. Tran IT, Sandy AR, Carulli AJ, Ebens C, Chung J, Shan GT, et al. Blockade of individual Notch ligands and receptors controls graft-versus-host disease. J Clin Invest. 2013; 123(4):1590–1604. [PubMed: 23454750]
23. Sandy AR, Chung J, Toubai T, Shan GT, Tran IT, Friedman A, et al. T cell-specific notch inhibition blocks graft-versus-host disease by inducing a hyporesponsive program in alloreactive CD4+ and CD8+ T cells. J Immunol. 2013; 190(11):5818–5828. [PubMed: 23636056]
24. Roderick JE, Gonzalez-Perez G, Kuksin CA, Dongre A, Roberts ER, Srinivasan J, et al. Therapeutic targeting of NOTCH signaling ameliorates immune-mediated bone marrow failure of aplastic anemia. J Exp Med. 2013; 210(7):1311–1329. [PubMed: 23733784]
25. Piggott K, Deng J, Warrington K, Younge B, Kubo JT, Desai M, et al. Blocking the NOTCH pathway inhibits vascular inflammation in large-vessel vasculitis. Circulation. 2011; 123(3):309–318. [PubMed: 21220737]
26. Shi S, Stanley P. Protein O-fucosyltransferase 1 is an essential component of Notch signaling pathways. Proc Natl Acad Sci U S A. 2003; 100(9):5234–5239. [PubMed: 12697902]
27. Han H, Tanigaki K, Yamamoto N, Kuroda K, Yoshimoto M, Nakahata T, et al. Inducible gene knockout of transcription factor recombination signal binding protein-J reveals its essential role in T versus B lineage decision. Int Immunol. 2002; 14(6):637–645. [PubMed: 12039915]
28. Yang X, Klein R, Tian X, Cheng HT, Kopan R, Shen J. Notch activation induces apoptosis in neural progenitor cells through a p53-dependent pathway. Dev Biol. 2004; 269(1):81–94. [PubMed: 15081359]
29. Rubtsov YP, Rasmussen JP, Chi EY, Fontenot J, Castelli L, Ye X, et al. Regulatory T cell-derived interleukin-10 limits inflammation at environmental interfaces. Immunity. 2008; 28(4):546–558. [PubMed: 18387831]
30. Murtaugh LC, Stanger BZ, Kwan KM, Melton DA. Notch signaling controls multiple steps of pancreatic differentiation. Proc Natl Acad Sci U S A. 2003; 100(25):14920–14925. [PubMed: 14657333]
31. Hill JA, Feuerer M, Tash K, Haxhinasto S, Perez J, Melamed R, et al. Foxp3 transcription-factor-dependent and -independent regulation of the regulatory T cell transcriptional signature. Immunity. 2007; 27(5):786–800. [PubMed: 18024188]
32. Marson A, Kretschmer K, Frampton GM, Jacobsen ES, Polansky JK, MacIsaac KD, et al. Foxp3 occupancy and regulation of key target genes during T-cell stimulation. Nature. 2007; 445(7130): 931–935. [PubMed: 17237765]
33. Sugimoto N, Oida T, Hirota K, Nakamura K, Nomura T, Uchiyama T, et al. Foxp3-dependent and -independent molecules specific for CD25+CD4+ natural regulatory T cells revealed by DNA microarray analysis. Int Immunol. 2006; 18(8):1197–1209. [PubMed: 16772372]
34. Ouyang W, Beckett O, Flavell RA, Li MO. An essential role of the Forkhead-box transcription factor Foxo1 in control of T cell homeostasis and tolerance. Immunity. 2009; 30(3):358–371. [PubMed: 19285438]
35. Ouyang W, Liao W, Luo CT, Yin N, Huse M, Kim MV, et al. Novel Foxo1- dependent transcriptional programs control T(reg) cell function. Nature. 2012; 491(7425):554–559. [PubMed: 23135404]
36. Tejera MM, Kim EH, Sullivan JA, Plisch EH, Suresh M. FoxO1 controls effector-to- memory transition and maintenance of functional CD8 T cell memory. J Immunol. 2013; 191(1):187–199. [PubMed: 23733882]
37. Zheng Y, Josefowicz S, Chaudhry A, Peng XP, Forbush K, Rudensky AY. Role of conserved non-coding DNA elements in the Foxp3 gene in regulatory T-cell fate. Nature. 2010; 463(7282):808–812. [PubMed: 20072126]
38. Koch MA, Thomas KR, Perdue NR, Smigiel KS, Srivastava S, Campbell DJ. T-bet(+) Treg cells undergo abortive Th1 cell differentiation due to impaired expression of IL-12 receptor beta2. Immunity. 2012; 37(3):501–510. [PubMed: 22960221]

39. Koch MA, Tucker-Heard G, Perdue NR, Killebrew JR, Urdahl KB, Campbell DJ. The transcription factor T-bet controls regulatory T cell homeostasis and function during type 1 inflammation. Nat Immunol. 2009; 10(6):595–602. [PubMed: 19412181]
40. Bailis W, Yashiro-Ohtani Y, Fang TC, Hatton RD, Weaver CT, Artis D, et al. Notch simultaneously orchestrates multiple helper T cell programs independently of cytokine signals. Immunity. 2013; 39(1):148–159. [PubMed: 23890069]
41. Perumalsamy LR, Nagala M, Banerjee P, Sarin A. A hierarchical cascade activated by non-canonical Notch signaling and the mTOR-Rictor complex regulates neglect-induced death in mammalian cells. Cell death and differentiation. 2009; 16(6):879–889. [PubMed: 19265851]
42. Huang H, Tindall DJ. Regulation of FOXO protein stability via ubiquitination and proteasome degradation. Biochim Biophys Acta. 2011; 1813(11):1961–1964. [PubMed: 21238503]
43. Plas DR, Thompson CB. Akt activation promotes degradation of tuberin and FOXO3a via the proteasome. J Biol Chem. 2003; 278(14):12361–12366. [PubMed: 12517744]
44. Kerdiles YM, Stone EL, Beisner DR, McGargill MA, Ch'en IL, Stockmann C, et al. Foxo transcription factors control regulatory T cell development and function. Immunity. 2010; 33(6): 890–904. [PubMed: 21167754]
45. Floess S, Freyer J, Siewert C, Baron U, Olek S, Polansky J, et al. Epigenetic control of the foxp3 locus in regulatory T cells. PLoS biology. 2007; 5(2):e38. [PubMed: 17298177]
46. Ohkura N, Hamaguchi M, Morikawa H, Sugimura K, Tanaka A, Ito Y, et al. T cell receptor stimulation-induced epigenetic changes and Foxp3 expression are independent and complementary events required for Treg cell development. Immunity. 2012; 37(5):785–799. [PubMed: 23123060]
47. Oldenhove G, Bouladoux N, Wohlfert EA, Hall JA, Chou D, Dos Santos L, et al. Decrease of Foxp3+ Treg cell number and acquisition of effector cell phenotype during lethal infection. Immunity. 2009; 31(5):772–786. [PubMed: 19896394]
48. Zhou X, Bailey-Bucktrout SL, Jeker LT, Penaranda C, Martinez-Llordella M, Ashby M, et al. Instability of the transcription factor Foxp3 leads to the generation of pathogenic memory T cells in vivo. Nat Immunol. 2009; 10(9):1000–1007. [PubMed: 19633673]
49. Feuerer M, Hill JA, Kretschmer K, von Boehmer H, Mathis D, Benoist C. Genomic definition of multiple ex vivo regulatory T cell subphenotypes. Proc Natl Acad Sci U S A. 2010; 107(13):5919–5924. [PubMed: 20231436]
50. Li QZ, Zhou J, Wandstrat AE, Carr-Johnson F, Branch V, Karp DR, et al. Protein array autoantibody profiles for insights into systemic lupus erythematosus and incomplete lupus syndromes. Clin Exp Immunol. 2007; 147(1):60–70. [PubMed: 17177964]
51. Schmitt EG, Haribhai D, Williams JB, Aggarwal P, Jia S, Charbonnier LM, et al. IL-10 produced by induced regulatory T cells (iTregs) controls colitis and pathogenic ex-iTregs during immunotherapy. J Immunol. 2012; 189(12):5638–5648. [PubMed: 23125413]
52. Noval Rivas M, Burton OT, Wise P, Charbonnier LM, Georgiev P, Oettgen HC, et al. Regulatory T Cell Reprogramming toward a Th2-Cell-like Lineage Impairs Oral Tolerance and Promotes Food Allergy. Immunity. 2015; 42(3):512–523. [PubMed: 25769611]

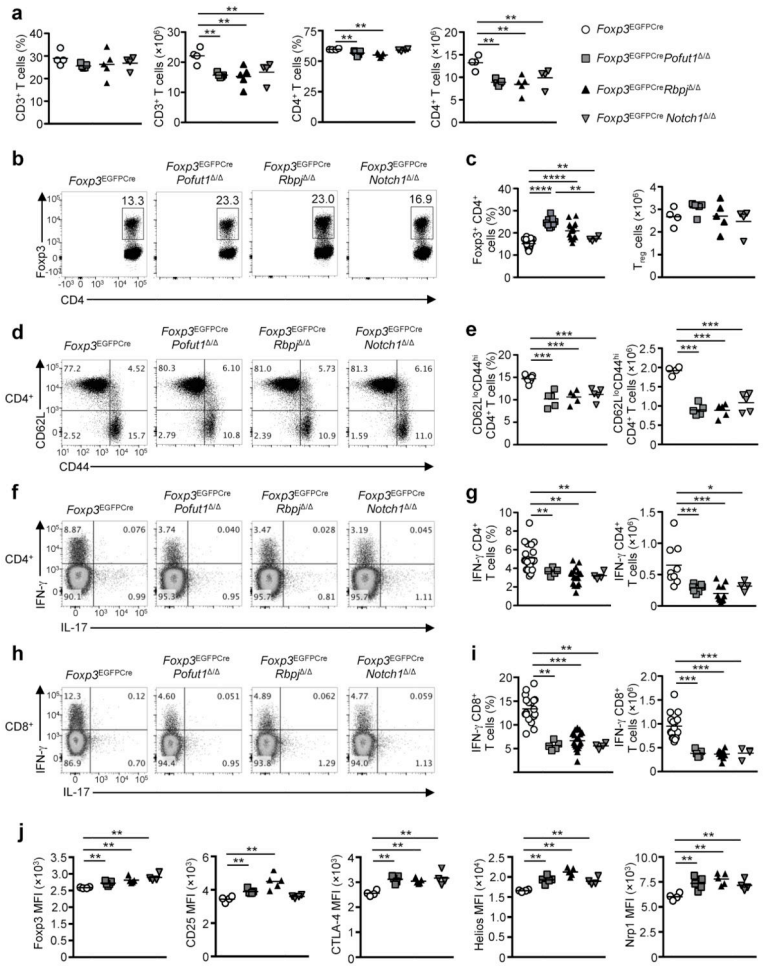

Fig. 1. Interruption of Notch signaling in T_{reg} cells results in a super-regulatory phenotype

(**a**) Frequencies and numbers of CD3 and CD4 T cells from the spleen of 8 weeks old *Foxp3*^{EGFPCre}, *Foxp3*^{EGFPCre}*Pofut*$^{\Delta/\Delta}$, *Foxp3*^{EGFPCre}*Rbpj*$^{\Delta/\Delta}$ and *Foxp3*^{EGFPCre}*Notch1*$^{\Delta/\Delta}$ mice. (**b**) Flow cytometric analyses of CD4 and Foxp3 markers on CD3$^+$ T cells are shown. (**c**) Frequencies and numbers of T_{reg} cells for each group of panel (a). (**d**) Flow cytometric analysis of CD62L and CD44 markers on CD4$^+$ T cells are shown. (**e**) Frequencies and numbers of memory CD4$^+$ T cells for each group. (**f**) Flow cytometric analyses of IFN-γ and IL-17 on CD4$^+$ T cells are shown. (**g**) Frequencies and numbers of IFN-γ producing CD4$^+$ T cells for each group. (**h**) Flow cytometric analyses of IFN-γ and IL-17 expression in CD8$^+$ T cells. (**i**) Frequencies and numbers of IFN-γ producing CD8$^+$ T cells shown in panel (H). (**j**) Expression of Foxp3, CD25, CTLA4, Helios and Nrp1 markers were evaluated of splenic T_{reg} cells and expressed as mean fluorescence intensity (MFI). Results are representative of at least 3 experiments per panel. * p<0.05, ** p<0.01, *** p<0.001 and **** p<0.0001 by one way ANOVA with post test analysis.

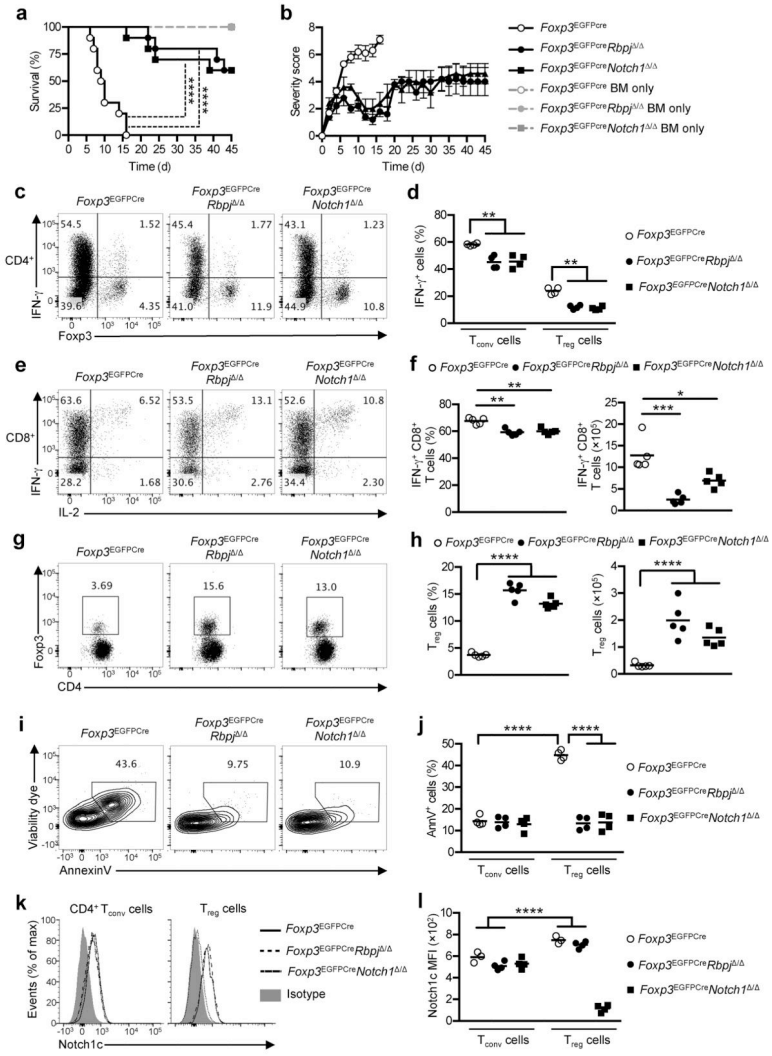

Fig. 2. T_{reg} cell-specific loss of function Notch signaling mutations protect mice from lethal graft versus host disease

(**a**) Survival and (**b**) severity score of lethally irradiated (8.5/9Gy) BALB/c mice infused with C57Bl/6 *Foxp3*^{EGFPCre}, *Foxp3*^{EGFPCre}*Rbpj*$^{\Delta/\Delta}$ or *Foxp3*^{EGFPCre}*Notch1*$^{\Delta/\Delta}$ T cell-depleted bone marrow, either alone (BM only) or together with spleen cells of the respective genotypes. For T cell subpopulation analyses were carried out on spleen cells at day 5 post adoptive transfer. The BM only groups were not included in panel b. (**c**) Flow cytometric analyses of IFN-γ and Foxp3 markers on CD4$^+$ T cells are shown. (**d**) Frequencies of IFN-γ producing CD4$^+$ T_{conv} (Foxp3$^-$) and T_{reg} (Foxp3$^+$) cells for each group. (**e**) Flow cytometric analyses of IFN-γ and IL-2 markers on CD8$^+$ T cells. (**f**) Frequencies and numbers of IFN-γ producing CD8$^+$ T cells for each group. (**g**) Flow cytometric analyses of Foxp3 marker on CD4$^+$ T cells are shown. (**h**) Frequencies and numbers T_{reg} cells for each group. (**i**) Viability dye and Annexin V (AnnV) staining of T_{reg} cells are shown (**j**) Frequencies of apoptotic (AnnV$^+$) T_{conv} and T_{reg} cells for each group. (**k**) Overlay of representative N1c expression on T_{conv} and T_{reg} cells are shown. (**l**) MFI of N1c expression in T_{conv} and T_{reg} cells for each group. Results are representative of at least 2 experiments per panel. * p<0.05, ** p<0.01,

*** $p<0.001$ and **** $p<0.0001$ by log-rank test, one way ANOVA and two way ANOVA with post test analysis.

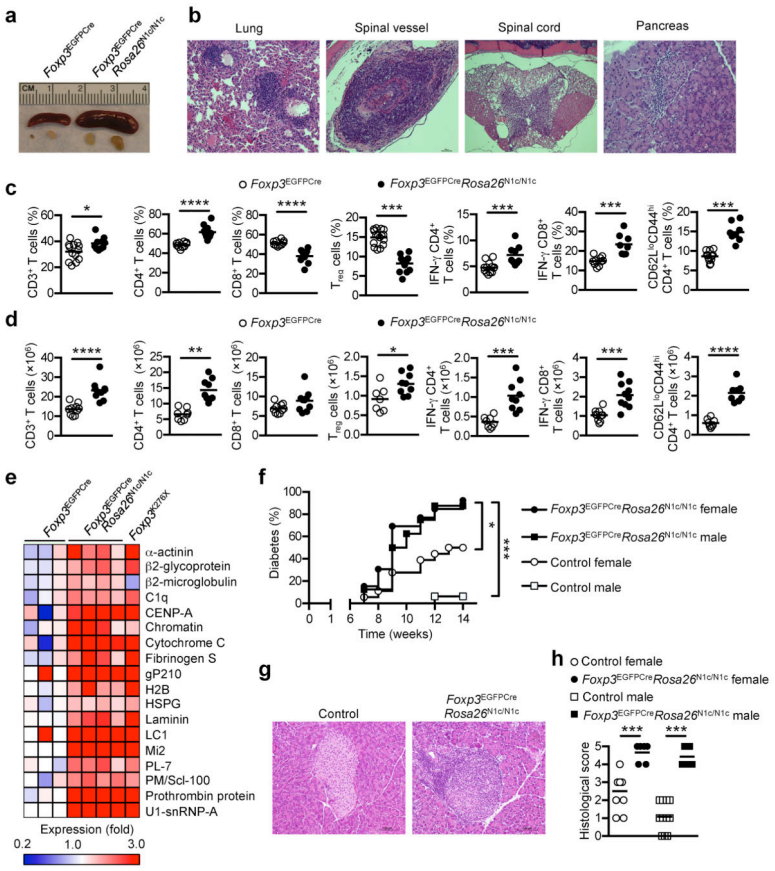

Fig. 3. Exacerbated Notch signaling in T_{reg} cells results in immune dysregulation and autoimmunity

(**a**) A representative picture of spleens and peripheral lymph nodes from 6 months old *Foxp3*^{EGFPCre} and *Foxp3*^{EGFPCre}*Rosa26*$^{N1c/N1c}$ mice. (**b**) Representative pictures of H&E staining of lung, spinal vessels, spinal cord and pancreas from 6 month old *Foxp3*^{EGFPCre}*Rosa26*$^{N1c/N1c}$ mice. Frequencies (**c**) and numbers (**d**) of CD3, CD4, CD8 T cells, T_{reg} cells, IFN-γ producing CD4 and CD8 T cells and memory CD62L^{lo}CD44^{hi} CD4 T cells from the spleen of 8 weeks old *Foxp3*^{EGFPCre} (white circles) and *Foxp3*^{EGFPCre}*Rosa26*$^{N1c/N1c}$ (black circles) mice. (**e**) Heatmap summarizing the expression of circulating autoantibodies significantly increased in 8 weeks old *Foxp3*^{EGFPCre}*Rosa26*$^{N1c/N1c}$ compared to *Foxp3*^{EGFPCre} mice (serum from *Foxp3*^{K276X} was used as a positive control). (**f**) Diabetes incidence of *littermate control* and *Foxp3*^{EGFPCre}*Rosa26*$^{N1c/N1c}$ female (n=18 and n=13 respectively) and male (n=16 and n=8 respectively) mice on NOD background. (**g, h**) Representative pictures of H&E staining of pancreas and histological score of 15 weeks old control females (white circles) or males (white squares) and *Foxp3*^{EGFPCre}*Rosa26*$^{N1c/N1c}$ females (Black circles) or males (black squares) on NOD background. * p<0.05, ** p<0.01, *** p<0.001 and **** p<0.0001 by unpaired two-tailed Student's *t*-test and log-rank test.

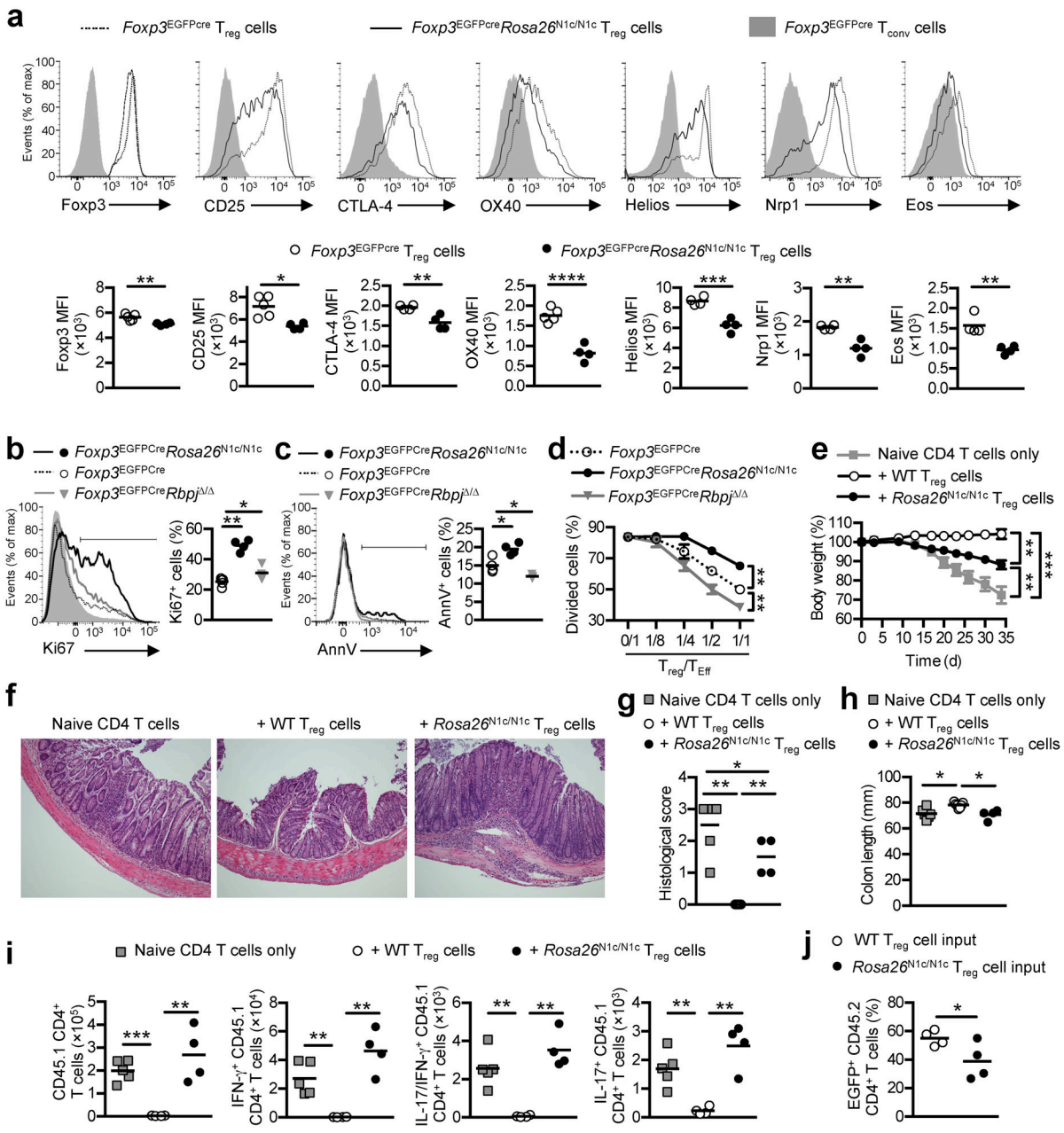

Fig. 4. Notch signaling compromises T_{reg} cell phenotype and suppressive functions

(a) Expression of Foxp3, CD25, CTLA4, OX40, Helios, Nrp1 and Eos markers were evaluated in splenic T_{reg} cells of *Foxp3*^{EGFPCre} (Dashes lines and white circles) and *Foxp3*^{EGFPCre}*Rosa26*$^{N1c/N1c}$ (Solid lines and black circles) mice. Gray plains represent expression of those markers in T_{conv} of *Foxp3*^{EGFPCre} mice. Cell turn-over was assessed in T_{reg} cells of *Foxp3*^{EGFPCre} (Dashes lines and white circles), *Foxp3*^{EGFPCre}*Rosa26*$^{N1c/N1c}$ (Solid black lines and black circles) and *Foxp3*^{EGFPCre}*Rbpj*$^{Δ/Δ}$ (Solid gray lines and Gray triangles) by Ki67 staining **(b)** for active cell cycle phases and by AnnV staining **(c)** for apoptosis. **(d)** *In vitro* suppression of responder CD4$^+$ T cell proliferation (T^{Eff}) was assessed by evaluation of proliferation dye dilution upon anti- CD3/C28 stimulation in the

presence of various number of T_{reg} cells from each genotype. *In vivo* suppressive capacity of T_{reg} cells from *Foxp3*^{EGFPCre} (white circles), *Foxp3*^{EGFPCre}*Rosa26*$^{N1c/N1c}$ (black circles) was assessed in the CD4 T cell transfer-induced colitis model. **(e)** Changes in body weight over time are shown (n=4–7). One representative experiment of 3 is shown. **(f–h)** Disease severity was evaluated by H&E staining of colon sections and end point colon length. **(i)** Absolute number of total, IFN-γ and IL-17-producing CD45.1^{+}CD4^{+} T cells from the naïve T cell input was quantified within the entire colon. **(j)** Stability of T_{reg} cell lineage was shown by percent of EGFP expression of the CD45.2 T cell compartment. * $p<0.05$, ** $p<0.01$, *** $p<0.001$ and **** $p<0.0001$ by unpaired two-tailed Student's *t*-test, One way ANOVA with post test analysis and two way ANOVA.

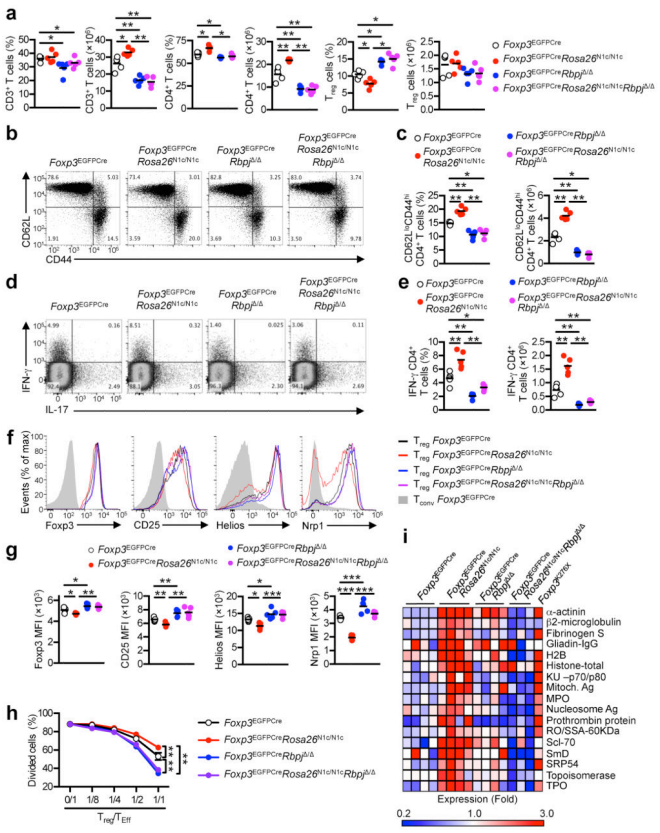

Fig. 5. T_{reg} cell failure and disease manifestations in *Foxp3*^{EGFPCre}*Rosa26*$^{N1c/N1c}$ mice proceed by a canonical pathway dependent mechanism

(a) Frequencies and numbers of CD3, CD4 and T_{reg} cells from the spleen of 8 weeks old *Foxp3*^{EGFPcre}, *Foxp3*^{EGFPCre}*Rosa26*$^{N1c/N1c}$, *Foxp3*^{EGFPCre}*Rbpj*$^{\Delta/\Delta}$ and *Foxp3*^{EGFPCre}*Rosa26*$^{N1c/N1c}$*Rbpj*$^{\Delta/\Delta}$ mice. **(b)** Flow cytometric analysis of CD62L and CD44 markers on $CD4^+$ T cells. **(c)** Scatter plots represent frequencies and numbers of memory $CD4^+$ T cells for each group. **(d)** Flow cytometric analysis of IFN-γ and IL-17 secretion by $CD4^+$ T cells are shown. **(e)** Scatter plots represent frequencies and numbers of IFN-γ producing $CD4^+$ T cells for each group. **(f, g)** Expression of Foxp3, CD25, Helios, Nrp1 markers were evaluated in splenic T_{reg} cells of each group. n=4–5 per group. **(h)** *In vitro* suppression of responder $CD4^+$ T cell proliferation (T^{Eff}) was assessed by evaluation of proliferation dye dilution upon anti-CD3/C28 stimulation in the presence of various number of T_{reg} cells from each genotype. **(I)** Heatmap summarizing the expression of significantly modulated circulating autoantibodies in 8 weeks old *Foxp3*^{EGFPCre}, *Foxp3*^{EGFPCre}*Rosa26*$^{N1c/N1c}$ and *Foxp3*^{EGFPCre}*RBPJ*$^{\Delta/\Delta}$ and *Foxp3*^{EGFPCre}*Rosa26*$^{N1c/N1c}$*Rbpj*$^{\Delta/\Delta}$ mice (serum from *Foxp3*^{K276X} was used as positive control). One representative experiment of 2 or 3 is shown for panels (a-h). * $p<0.05$ and ** $p<0.01$ by One way ANOVA with post test analysis and two way ANOVA.

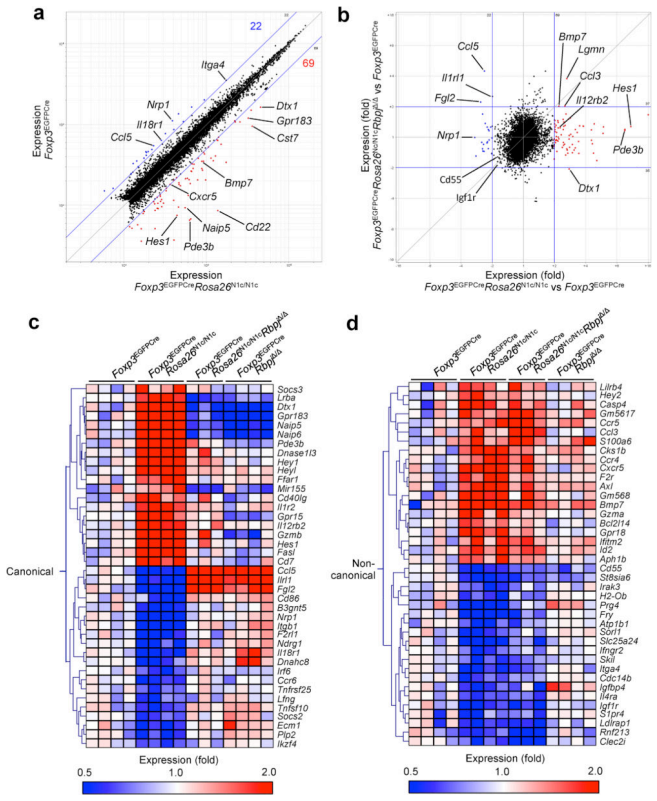

Fig. 6. Impact of Notch signaling on the T_{reg} cell transcriptome

(a) Microarray analysis of gene expression (mean) of *Foxp3*^{EGFPCre}*Rosa26*$^{N1c/N1c}$ (n = 4) (X axis) versus *Foxp3*^{EGFPCre} T_{reg} cells (n=4). Numbers in plots indicate total genes downregulated (red) or upregulated (blue) in N1c overexpressing T_{reg} cells relative to their expression in *Foxp3*^{EGFPCre} T_{reg} cells (cutoff of a two fold change). **(b)** Comparison of changes in gene expression induced by Notch1 signaling (*Foxp3*^{EGFPCre}*Rosa26*$^{N1c/N1c}$ vs *Foxp3*^{EGFPCre}; horizontal axis) and those induced by Notch gain of function in absence of canonical pathway (*Foxp3*^{EGFPCre}*Rosa26*$^{N1c/N1c}$*Rbpj*$^{\Delta/\Delta}$ vs *Foxp3*^{EGFPCre}; vertical axis) within T_{reg} cells. Blue lines mark a fold change of 2. **(c, d)** Genes whose expressions are significantly modulated ($p<0.05$ by one way ANOVA) were segregated in 2 clusters based on the pattern of modulation (canonical and non-canonical) and representative heat maps for each cluster are shown.

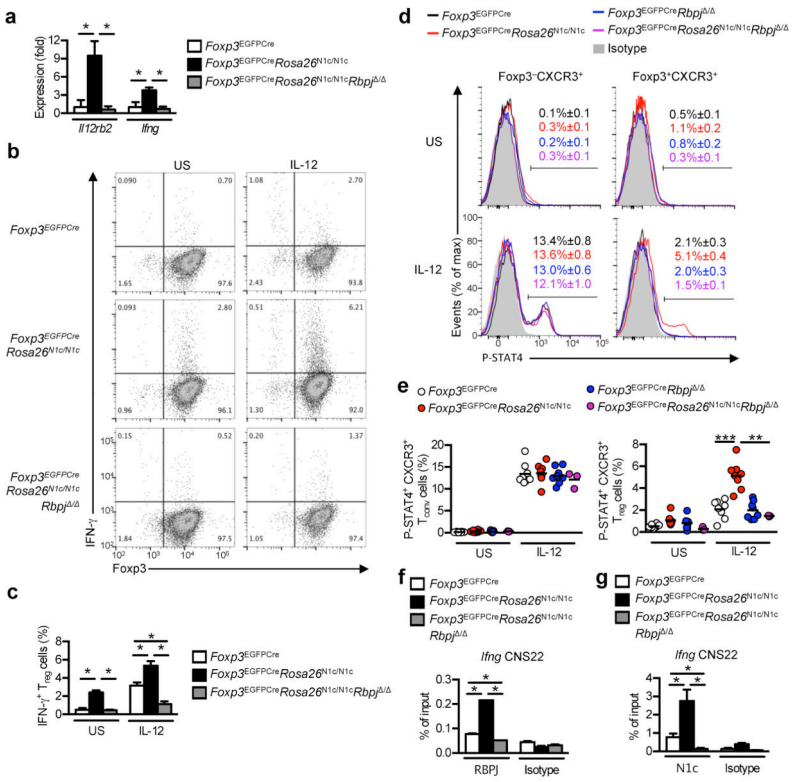

Fig. 7. N1c mediates T_H1 reprogramming of T_{reg} cells

(a) qPCR analysis of *Il12rb2* and *Ifng* transcripts in T_{reg} cells isolated from *Foxp3*^{EGFPCre}, *Foxp3*^{EGFPCre}*Rosa26*$^{N1c/N1c}$ and *Foxp3*^{EGFPCre}*Rosa26*$^{N1c/N1c}$*Rbpj*$^{Δ/Δ}$ mice (n=4–6 per group). Results represent mean fold change + S.E.M. compared to mean of *Foxp3*^{EGFPCre} T_{reg} cells. Representative flow cytometry dot plots **(b)** and histograms **(c)** of IFN-γ production by sorted T_{reg} cells after ex-vivo IL-12 stimulation (n=3 per group). Representative histograms **(d)** and dot plots **(e)** of P-STAT4 on gated Foxp3^{-}CXCR3^{+} and CD4^{+}Foxp3^{+}CXCR3^{+} cells after CD4 enrichment and IL-12 stimulation (n=3–8 per group). ChIP graphs represent quantitative PCR analysis of the ratio of enriched *Ifng* CNS22 binding site immuneprecipitated with anti-RBPJ **(f)** and anti-N1c **(g)** to the input DNA on T_{reg} cells isolated from *Foxp3*^{EGFPCre}, *Foxp3*^{EGFPCre}*Rosa26*$^{N1c/N1c}$ and *Foxp3*^{EGFPCre}*Rosa26*$^{N1c/N1c}$*Rbpj*$^{Δ/Δ}$ mice (n=3 per group). * p<0.05, ** p<0.01 and *** p<0.001 by unpaired two-tailed Student's *t*-test and One Way ANOVA with post test analysis.

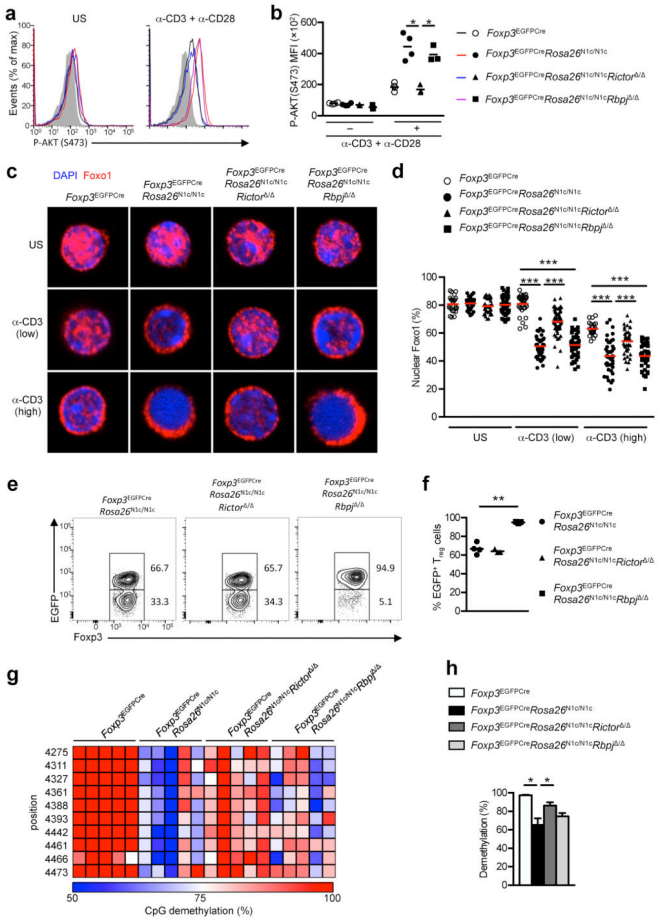

Fig. 8. Rictor-dependent non-canonical signaling dysregulates AKT-Foxo1 axis in *Foxp3*^{EGFPCre}*Rosa26*$^{N1c/N1c}$ T$_{reg}$ cells

(**a**) Flow cytometric analysis and (**b**) scatter plot analysis of MFI of unstimulated and anti-CD3/anti-CD28 stimulated T$_{reg}$ cells from *Foxp3*^{EGFPCre}, *Foxp3*^{EGFPCre}*Rosa26*$^{N1c/N1c}$, *Foxp3*^{EGFPCre}*Rosa26*$^{N1c/N1c}$*Rictor*$^{\Delta/\Delta}$ and *Foxp3*^{EGFPCre}*Rosa26*$^{N1c/N1c}$*Rbpj*$^{\Delta/\Delta}$ mice. (**c**) N1c augments anti-CD3 mAb-induced translocation of nuclear Foxo1 to the cytosol in a Rictor dependent manner. Unstimulated and anti-CD3 mAb stimulated T$_{reg}$ cells were stained for nuclear DNA (DAPI) and Foxo1 and examined by confocal microscopy for Foxo1 distribution in the nucleus vs. cytosol. (**d**) Quantitation of percent Foxo1 nuclear expression. Each point represents one cell. (**e**) Flow cytometric analyses of Foxp3 and EGFP expression in peripheral T$_{reg}$ cells from *Foxp3*^{EGFPCre}*Rosa26*$^{N1c/N1c}$, *Foxp3*^{EGFPCre}*Rosa26*$^{N1c/N1c}$*Rictor*$^{\Delta/\Delta}$ and *Foxp3*^{EGFPCre}*Rosa26*$^{N1c/N1c}$*Rbpj*$^{\Delta/\Delta}$ mice. (**f**) Fractions of EGFP^{+} cells among Foxp3^{+} T$_{reg}$ cells from panel (e). (**g**) Methylation status of individual CpG motifs within the TSDR of *CNS2* in *Foxp3*. Individual CpG motifs are numbered with reference to the transcription initiation site of Foxp3. (**h**) Global methylation status of the TSDR of *CNS2* in *Foxp3*. * p<0.05, ** p<0.01 and *** p<0.001 by unpaired two-tailed Student's *t*-test and One Way ANOVA with post test analysis.